inventions

Article

The Influence of Nusselt Correlation on Exergy Efficiency of a Plate Heat Exchanger Operating with TiO_2:SiO_2/EG:DI Hybrid Nanofluid

Sylwia Wciślik

Department of Building Physics and Renewable Energy, Faculty of Environmental Engineering, Geodesy and Renewable Energy, Kielce University of Technology, Aleja Tysiaclecia Panstwa Polskiego 7, 25-314 Kielce, Poland; sylwiazw@tu.kielce.pl

Abstract: This paper studies how the correlation with the Nusselt number affects the final result of the efficiency, ε, and exergy efficiency, η_{ex}, of a chevron-type gasketed plate heat exchanger, which is installed in a typical small solar installation dedicated to single-family housing; the solar fluid is a TiO_2:SiO_2/EG:DI hybrid nanofluid with concentrations from 0% to 1.5% vol. The experimental model assumes constant flow of the solar fluid and varies on the domestic hot water side—from 3 lpm to 6 lpm. The inlet temperatures are 30 °C and 60 °C on the cold and hot sides of the heat exchanger, respectively. Of the six analysed correlations that showed similar trends, it is concluded that for the assumed flow conditions, geometry, and chevron angle of the plate heat exchanger, one model is the most accurate. The largest difference between the η_{ex} values for a given concentration is 3.4%, so the exergy efficiency is not affected by the chosen Nusselt model by very much. However, the choice of correlation with the Nusselt number significantly affects the efficiency, ε; the difference between the values obtained within a given concentration is more than 40% and depends on the Reynolds number and flow. Most research discusses the scenario with the nanofluid as a coolant. This paper considers the opposite situation in which the solar fluid is a hotter working medium that transfers heat to domestic hot water installation.

Keywords: nanofluids; heat exchanger modelling; Nusselt number correlation; heat transfer enhancement

check for updates

Citation: Wciślik, S. The Influence of Nusselt Correlation on Exergy Efficiency of a Plate Heat Exchanger Operating with TiO_2:SiO_2/EG:DI Hybrid Nanofluid. *Inventions* **2024**, *9*, 11. https://doi.org/10.3390/inventions9010011

Academic Editor: Shyy Woei Chang

Received: 7 December 2023
Revised: 2 January 2024
Accepted: 4 January 2024
Published: 9 January 2024

1. Introduction

Nowadays, much attention is paid to environmental aspects, sustainable development, and energy efficiency [1]. Therefore, the role of heat exchangers, especially in HVAC (heating, ventilation, and air conditioning) installations, is becoming more important. These devices make it possible to improve the efficiency of systems by using and reusing, for example, waste heat. Additionally, heat exchange between two fluids with different thermodynamic parameters takes place in a non-contact manner. Intensive research is also carried out on working fluids whose thermodynamic potential and heat capacity allow for even more effective heat exchange or cold recovery [2]. The new generation of working fluids cooperating with heat exchangers undoubtedly includes mono- and hybrid nanofluids of various concentrations. The most famous and tested heat exchangers include double-tube heat exchangers [3], plate heat exchangers (PHEs) [4], and shell and tube heat exchangers [5]. By entering the two terms 'nanofluids' + 'heat exchangers' in the search engine on the ScienceDirect platform, a total of 12,859 publications of various types are obtained; the first dates back to 1998 [6]. Among the types of publications available in Scopus, the most common are research articles, 78.6%; followed by review articles, 10%; short communications, 4.5%; and book chapters, 3.3%. The remainder constitutes approximately 3%, including conference abstracts, encyclopaedia, case reports, editorials, mini reviews, correspondence, news, and other types (see Figure 1). Furthermore, up to

63% of the publications concern PHEs. And, this type of exchanger is also the subject of this paper.

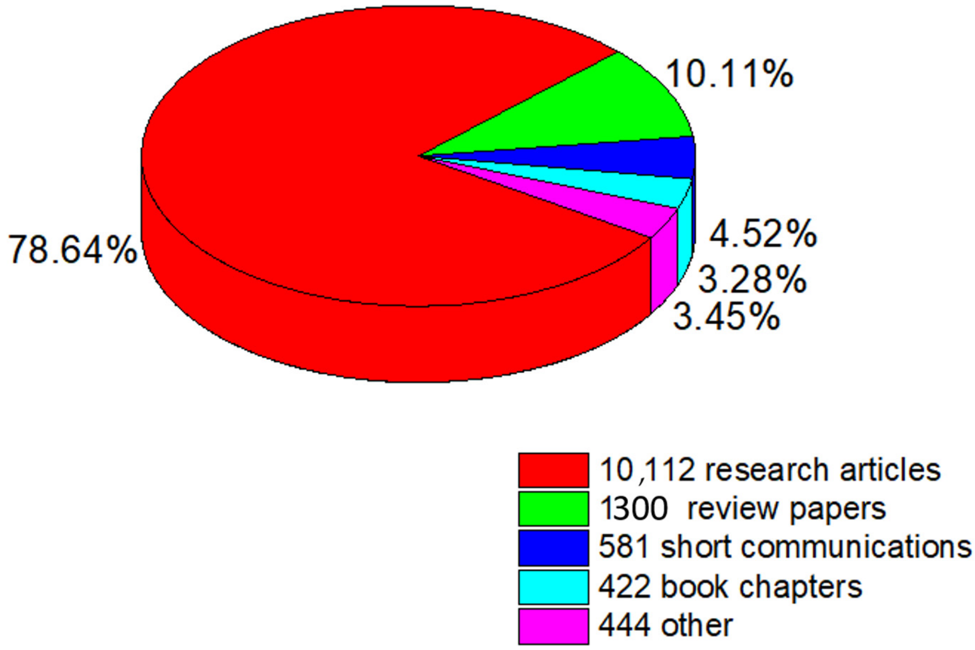

Figure 1. The number of publications registered in the Scopus database for the entries 'nanofluids' + 'heat exchangers' from 1999 to 22 September 2023.

The most common analysis in the literature concerns the efficiency of PHEs operating with nanofluids on the secondary side of the installation [2–5]. This means that the heat-receiving factor is a suspension of various concentrations, produced on the basis of deionised water [7], and mixtures of water with glycols [8] or oils [9]. The methods of producing and stabilising nanofluids are described in detail in [10], and the basic limitations and requirements include, among others, economic considerations or problems with increasing pumping power in [11–13]. The use of nanofluids is extremely effective due to their proven superior thermal and rheological properties [14]. The thermal conductivity coefficient can be from several (0.25% $CaCO_3$(50:50%)/DI [15] or 0.3% Fe_3O_4–CNT/water [16]) to even several dozen percents higher (1% TiO_2 + MWCNT/EG [17] and 1.5% Al_2O_3 + MWCNT/thermal oil [9]) than in the case of the base liquid. Nanofluids are also eagerly tested in closed-loop solar systems [18], in which solar radiation energy is converted into thermal [19] or electrical energy [20]. The efficiency of exchanger installations can be effectively determined using the exergy method, as in, for example, [21–23]. Iranmanesh et al. in [24] showed that graphene nanoplatelets (water-based) nanofluids with a concentration of 0.1% wt. in a solar installation with a PHE will increase the exergy and thermal efficiencies by approximately 40% and 20%, respectively, compared to distilled water; the flow of working fluid was (1.5 dm^3/min).

The algorithm to determine the exergy efficiency of the plate heat exchanger requires, among others, assuming the appropriate correlation to the Nusselt number, Nu. It is directly related to other similarity numbers such as the Reynolds number, *Re*, or Prandtl number, *Pr*, with $Nu = f(Re, Pr)$, and allows us to calculate the heat transfer coefficient, h (see Equation (1)) [25]. The Nu number is the quotient of the thermal energy exchanged by convection with the conduction energy, which is generally written as Equation (2). Table 1 presents the universal, most known and proven functional relationships for the Nu number, which are used by researchers around the world to analyse laminar [26] and turbulent [27] flows, including nanofluids, but without taking into account their concentration and the type of nanoadditives. Some correlations take into account the influence of liquid viscosity [27–29], while others do not [30,31]. The Nusselt number should be calculated separately for each side of the plate heat exchanger, i.e., for the working medium with different flows and temperatures, in the hot and cold channels, respectively. In [27], Akturek et al. performed a new Nusselt correlation for the gasket type of PHE with a chevron angle of 30° and a heat transfer/extended surface area of 0.14 m^2. The counterflow water is maintained in the range of 0.57–6.6 m^3/h, on both the cold and hot sides, and the respective temperatures are T_c = 9–25 °C and T_h = 53–90 °C. An uncertainty analysis of the basic experimental parameters are as follows: for the Reynolds number, $u(Re)$ = 4.16; for the Nusselt number, $u(Nu)$ = 1.83; for the Prandtl number, $u(Pr)$ = 2.19; for heat transfer, $u(Q)$ = 0.40; for the overall heat transfer coefficient, $u(U)$ = 0.41; for the mean logarithmic temperature, u(LMTD) = 0.01; and for the friction factor, $u(f)$ = 4.18.

Table 1. General Nusselt number correlations for the chevron type of PHE.

Model Author	Nusselt Correlation	Reynolds Number Range	HE Type	Remarks
Akturk et al. [27]	$Nu = 0.32673\, Re^{0.6125} Pr^{1/3} \left(\frac{\mu_b}{\mu_w}\right)^{0.14}$	$Re = 450 - 5250$	gasketed-PHE	A = 0.14 m^2, β = 30°, $u(Nu)$ = 1.83%, water as operation fluid; 0.57–6.6 m^3/h, T_h = 53–90 °C, T_c = 9–25 °C; counterflow
Sieder and Tate [28]	$Nu = 1.86 \left(RePr\frac{D_h}{L_p}\right)^{1/3} \left(\frac{\mu_b}{\mu_w}\right)^{-0.14}$	$\left(RePr\frac{D_h}{L_p}\right)^{1/3} > 2$ $Re < 2100$	PHE and tube and shell and tube	$0.6 < Pr < 5$ $0.0044 < \frac{\mu_b}{\mu_w} < 9.75$ Oil and water as working fluids; for other fluids applicable as well; counterflow $T_{h,c}$ = 71.6–171 °C
Kumar et al. [29]	$Nu = 0.348\, Re^{0.663} Pr^{1/3} \left(\frac{\mu_b}{\mu_w}\right)^{0.17}$	$Re > 10$	PHE, commercial plates	β = 30–60° water, oils
Focke et al. [30]	$Nu = 1.112\, Re^{0.6} Pr^{0.5}$	$600 < Re < 16{,}000$	Models of PHE corrugated field	No data of Pr and mass transfer β = 80°, 70°, 60°, 45°, 30°; γ = 1.0; b = 5.0 mm $u(Nu)$ = 6.5%; $u(f)$ = 3.98% water, air
	$Nu = 0.57\, Re^{0.7} Pr^{0.5}$	$150 < Re < 600$		
Okada et al. [31]	$Nu = 0.1528\, Re^{0.66} Pr^{0.4}$	$400 < Re < 15{,}000$	PHE	β = 15°, 30°, 45°, 60° $u(Nu)$ = 30%

Proposed by Akturek et al. [27], the correlation for Nu is compared with other similar patterns, and the best fit is noted for Kumar et al. [29].

A very old correlation from 1936 given by Sieder and Tate in [28] originally for tubular-type water heat exchangers has also been used in nanofluids, e.g., by Alklaibi et al. [4], who investigated the cooling properties of hybrid nanofluids when flowing through the PHE.

For new and more accurate models, the Kumar et al. [29] correlation for the Nusselt number is recommended by [32,33].

The correlation given by Okada et al. [31] gives Nu values with even more than a 30% difference from other studies [27,34].

$$h = \frac{Nu\, k}{D}, \tag{1}$$

where k is the conductive heat transfer coefficient of the fluid, Nu is the Nusselt number describing the phenomenon of dynamic similarity, and D refers to the hydrodynamic channel diameter.

$$Nu = \frac{E_{conv}}{E_{cond}} = \frac{h\, D}{k}, \tag{2}$$

where E_{conv}, E_{cond} are thermal energy exchanged by convection and conduction, respectively.

It should also be noted that for precisely defined experimental conditions of flow and temperature, correlations with the Nu number are also suggested, which are true for a specific nanofluid and concentration range. Models like this take into account very precisely defined thermodynamic parameters of the working medium, such as the conductivity of nanoparticles and the base liquid, as well as their density and specific heat (see Equation (3)).

Yashawantha et al., in [35], developed a new correlation (see Equation (4)), which was checked for nanofluid temperatures, with $T_{nf,in}$ in the range from -5 up to +20 °C. On the other side of the heat exchanger, the temperature of the working medium was $T_{h,in}$ = 60 °C. The experiment used a 0.2–2% wt. Al_2O_3 nanofluid produced on the basis of a mixture of deionised water and ethylene glycol in a weight ratio of 65:35. Ultimately, a good agreement with the experimental data was obtained. The presence of nanoadditives resulted in an increase in heat transfer rate by a maximum of 5.07% (for a nanofluid concentration of 2%) compared to the base liquid; the overall heat transfer coefficient, U, increased by a maximum of 14.99%; the effectiveness, e, increased by 5.18%; and the power requirement for pumping, dp, increased by 13.74% (for a concentration and a temperature of nanofluid at 2% and $T_{nf,in}$ = -10 °C). The performance index was above unity, hence the conclusion that nanofluids are useful for practical and commercial use. The coefficient of determination was given as R^2 = 0.98.

$$Nu = f\left(Re, Pr, \varphi, \frac{k_{np}}{k_{bf}}, \frac{\rho_{np}c_{np}}{\rho_{nbf}c_{bf}}\right), \tag{3}$$

where φ is the volume or weight concentration of the suspension; k is the thermal conductivity; c is the specific heat; and indexes nf and bf refer to the nanoparticles and the base liquid, respectively.

$$Nu = aRe^m Pr^n \left(1 + \frac{\varphi}{100}\right)^b, \tag{4}$$

where, a, b, m, and n are the constants received from the regression analyses and depend on the nanofluid inlet temperature, φ is concentration, and the range of validated Reynolds number is $Re_{nf,c}$ = 100–200 (2–4 lpm).

In [36], local Nusselt number correlations for the heat transfer of nanofluids using genetic programming were proposed. It turns out that the variables that determine the Nusselt number are primarily the Re and Pr numbers, and the presence of nanoparticles affects the flow inertia forces and the thermal diffusivity. Many research and numerical works on nanofluids include Nusselt number correlations, which were validated for a specific flow range, i.e., the Re number. Most publications are concerned with the turbulent flow of nanofluids, e.g., in a circular tube [37–39]. Relatively few works have concerns about the low Reynolds number range, e.g., during the flow of nanofluids in micro heat sinks [8], through the PHE [35], or just in the pipe [40]. Lai et al. in [40] investigated an Al_2O_3-water nanofluid during laminar flow (Re < 270) in a millimetre-sized stainless steel tube. They showed an improvement in Nusselt number of about 8%. This research was conducted with a nanoparticle volume fraction of 0–1% and a size of 20 nm. Table 2 lists exemplary and more well-known correlations of the Nusselt number for nanofluids and the validation range.

Optimising the operation of exchanger systems involves selecting the output parameters so that their operation is highly efficient and energy-saving [41,42]. This often requires checking and applying specific solutions provided in the literature, such as correlations with the Nusselt number. Indirectly, it enables the calculation of many parameters related to heat transfer and the effective design of a given process. Therefore, this work attempts to analyse the impact of the adopted correlation on the Nusselt number on the final result of the efficiency, ε, and exergy efficiency, η_{ex}, of the PHE working in a typical solar installation. The atmospheric conditions of the experimental system also deserve attention. Most research studies that calculate the efficiency of the PHE assume that the nanofluid works on the secondary side of the plate heat exchanger as a coolant. This article assumes the opposite situation. The TiO_2:SiO_2 hybrid nanofluid with a concentration in the range of 0.5–1.5% is a solar fluid that circulates in the hot water installation on the primary side (that is, outside) of the PHE. The nanofluid is produced on the basis of ethylene glycol. This scenario occurs for installations located in countries where external air temperatures are low enough to cause the solar fluid to freeze, e.g., in central European countries. In this work, it is assumed that the heat from the solar installation will be transferred to the internal domestic water installation with an initial temperature of $T_{c,in}$ = 30 °C; the initial temperature of the working medium on the primary side is $T_{nf,in}$ = 60 °C. This paper also validates the research methodology for other publications.

Table 2. Nusselt number correlations for nanofluids.

Author	Nanoadditive/Base Fluid/Capacity	Nusselt Correlation	Reynolds Range	Remarks
Vajjiha et al. [37]	SiO_2/60:40 EG:DI, CuO/60:40 EG:DI nanofluids: 0 < f < 0.06%; A_12O_3/60:40 EG:DI nanofluid: 0 < f < 0.1 (Al_2O_3-45 nm, CuO-29 nm, SiO_2-20, 50, 100 nm)	$Nu_{nf} = 0.065\left(Re^{0.65} - 60.22\right)\left(1 + 0.0169\varphi^{0.15}\right)Pr^{0.542}$	3000 < Re < 6000	R^2 = 0.97 SD_{max} = 10% $u \pm 2\%$
Xuan and Li [38]	Cu/DI nanofluid f < 2% vol. Cu < 100 nm (vol. fraction: 0.3, 0.5, 0.8, 1, 1.2, 1.5, 2%)	$Nu_{nf} = 0.0059\left(1.0 + 7.6286\varphi^{0.6886}Pe_{dp}^{0.001}\right)Re_{nf}^{0.9238}Pr_{nf}^{0.4}$	10,000 < Re < 25,000	$u(dNu/Nu)$ < 4%
Xuan and Li [39]	Cu/DI nanofluid f < 2% vol. Cu < 25 nm (vol. fraction: 0.5, 1, 1.5, 2%)	$Nu_{nf} = 0.4328\left(1.0 + 11.285\varphi^{0.754}Pe_{p}^{0.218}\right)Re_{nf}^{0.333}Pr_{nf}^{0.4}$	200 < Re < 2000 (laminar flow)	
Jafarimoghaddam and Aberoumand [8]	Cu/oil nanofluid (wt. fraction: 0.12, 0.36, 0.72%)	$Nu_{nf} = 1.7Re^{0.136}Pr^{0.8}(0.003\varphi + 0.4)$	Re < 160 (laminar flow)	$u \pm 10\%$
Yashawantha et al. in [35]	Al_2O_3/65:35 EG:DI (wt. fraction: 0.2–2%)	$Nu_{nf} = aRe^{m}Pr^{n}\left(1 + \frac{\varphi}{100}\right)^{b}$	100 < Re < 200 (laminar flow); $T_{nf,in}$ = −5–10 °C, a = 0.287–0.767, b = 5.642–11.09, m = 0.454–0.657, n = 0.909–0.153	R^2 = 0.98 u < 6%

2. Thermal Performance Analysis

Due to that this paper being a numerical study, the operation of the heat exchanger was modelled in MATLAB. This experimental modelling concerns determining the efficiency of heat exchange with countercurrent flow of heating and heated liquids by a plate heat exchanger installed in a solar installation for preparing domestic hot water for a single-family residential building. It is assumed that the device is made of stainless steel with the dimensions given in Table 3 and Figure 2.

The technical parameters of the plate heat exchanger and its area are given in Table 3, and they are initial conditions. Heat exchangers of similar size and structure are commonly used in industry. The purpose of this work is not strictly to determine the size of the heat exchanger, but of course, it is possible. On the one hand, the total heat transfer surface area (A) can be estimated based on the known relationship, assuming the logarithmic mean temperature (ΔT_{LM}) and the overall required heat transfer coefficient (U); $A = Q/(U\ \Delta T_{LM})$. On the other hand, the plate surface area increases with corrugations on plates, which further leads to high heat transfer. The ratio of effective area to projected area of the plate is defined as the surface enlargement factor (Equations (5)–(9)), and for commercial plates, it generally ranges from 1.15 to 1.25.

Table 3. Technical parameters of the studied plate heat exchanger.

Technical Parameter of PHE	Symbol	Value
Plate width between gaskets	L_w, m	0.18
Plate height between ports	L_v, m	0.48
Plate height between gaskets	L_p, m	0.357
Plate width between ports	L_h, m	0.06
Port diameter	D_p	30
Chevron angle	β, °	30
Enhancement factor	ϕ	1.15
Surface area/heat transfer area	A, m^2	0.3
Corrugation pitch	P_c, mm	14.2
Mean channel spacing	b, mm	2.8
Plate pitch	p, mm	2.8
Plate thickness	t, mm	0.45
Total number of plates	N_t	6
Pass number	N_p	3
Thermal conductivity	k_p, W/mK	9.5

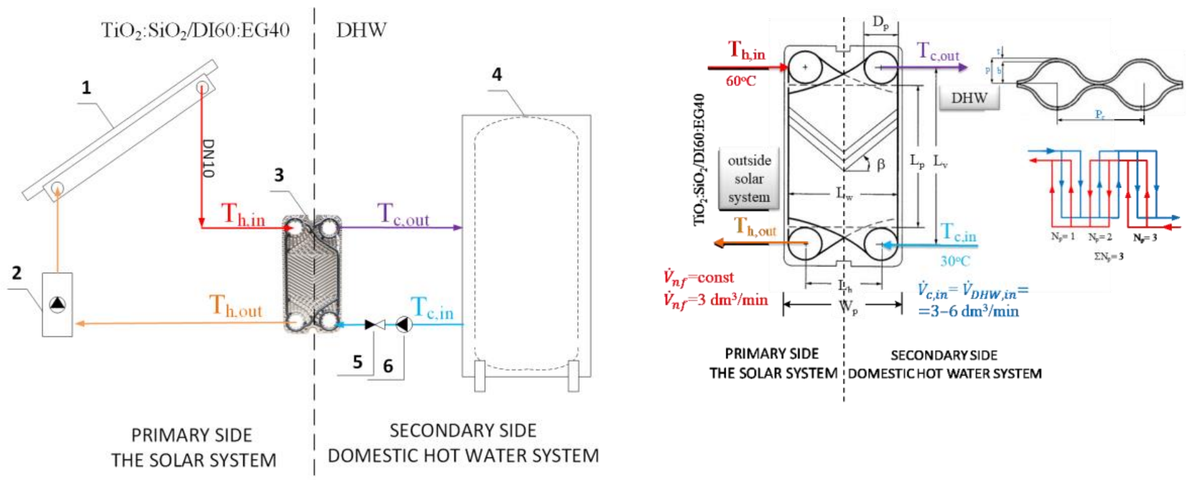

(**a**) (**b**)

Figure 2. (**a**) The hydraulic scheme of the solar system including the plate heat exchanger and operating conditions; (**b**) initial conditions of the solar system and basic dimensions of a chevron-type PHE with its cross-section dimensions normal to the direction of troughs.

$$\varphi = \frac{Effective\ area}{Projected\ area} = \frac{A_E}{A_P} \tag{5}$$

$$A_P = L_P\, w_P \tag{6}$$

$$A_E = \varphi\, L_P\, w_P \tag{7}$$

$$L_P = L - d_P \tag{8}$$

$$w_P = w - d_P \tag{9}$$

where L and w are the plate length and plate width, respectively; L_p and w_p are the projected length and projected width between the inlet and outlet ports; and d_p is the port diameter.

The enlargement factor of corrugation can also be determined as follows [43,44]:

$$\varphi = \frac{1}{6}\left[1 + \sqrt{1 + \left(\frac{\pi\gamma}{2}\right)^2} + 4\sqrt{1 + 0.5\left(\frac{\pi\,\gamma}{2}\right)^2}\right] \tag{10}$$

where γ is a channel profile aspect ratio.

The solar fluid in this case is a $TiO_2 + SiO_2$ hybrid nanofluid with a concentration in the range of 0.5–1.5% vol.; the base liquid is a mixture of deionised water and bioethylene glycol in the DI:EG ratio 60:40. The thermodynamic properties of the working medium are presented in Table 4; the values come from our own research and are very close to that presented in the literature [45]. Moreover, the initial conditions are also given in Figure 2. On the solar liquid side, under the operating conditions of the installation, the flow should be constant and the value recommended by [46] is 3 dm^3/min; while on the hot water side, it is the result of the current hot water consumption and ranges from 3 to 6 dm^3/min (which corresponds to the water outflow from the draw valve). The heat transfer was performed by modelling within MATLAB.

Table 4. Thermodynamic parameters of working fluids.

Working Fluid	0.5–1.5% Vol. TiO_2:SiO_2/DI:EG 60:40	DI:EG 60:40	DI
	Primary Side of PHE		Secondary Side of PHE
T_{in}, °C	60		30
$\dot{V}_{wf}$, dm^3/min	$\dot{V}_{nf}$ = const = 3		3–6
k, W/mK	0.468–0.470 *,*2	0.449	0.6
μ, Pa s	0.00161–0.00184 *,*3	0.00136	0.00080
ρ, kg/m^3	1024.38–1040.38 *,*4	1011.87	995.77
c, J/kgK	3956–3877 *,*4	3991.00	4178.97

* depends on the concentration/vol. fraction of nanoadditives; *2 C-Therm TCi Thermal Analyzer, accuracy of 5%; *3 RheolabQC rotational rheometer, resolution 2 µrad; *4 calculated on the basis of the rule of mixtures.

3. Methodology

The exergy efficiency [47] of the PHE is defined as the ratio of useful exergy output to total exergy input and can be written as follows:

$$\eta_{exergy} = 1 - \frac{T_a\,\dot{S}_{gen}}{\left(1 - \left(\frac{T_a}{T_{w,ex}}\right)\right)\dot{Q}_h}, \tag{11}$$

where T_a and $T_{w,ex}$ are the ambient and external surface temperatures of the PHE, respectively; $\dot{S}_{gen}$ is the total entropy generation of the fluid (see Equation (12)) that is a sum of thermal $\dot{S}_{gen,th}$ and friction $\dot{S}_{gen,\,fr}$ entropy; and $\dot{Q}_h$ is the heat transfer rate on the hot fluid side.

$$\dot{S}_{gen} = \frac{\dot{Q}_{av}^{\,2}}{Nu\;Re\;Pr\;T_{in}\;T_{out}\;L_v} + \frac{8f\dot{m}^2 L_v}{\rho^2\pi^2 D_h^2 (T_{out} - T_{in,})}\ln\left(\frac{T_{out}}{T_{in,}}\right), \tag{12}$$

where $\dot{Q}_{av}$ is the actual, average heat flux; T_{in}, T_{out} are the temperatures of the working fluid during input and output to and from the heat exchanger; L_v is the height of the PHE; ρ is the density; and f is the friction factor.

Then, based on Equations (13) and (14), the Reynolds and Prandtl numbers were calculated separately for fluids in the cold and hot channels of the studied PHE.

$$Re = \frac{\mathrm{GD_h}}{\mu}, \tag{13}$$

$$Pr = \frac{\mu c}{k}, \tag{14}$$

where G is the mass velocity; D_h is the hydraulic diameter that includes a mean channel gap b and enlargement factor ϕ, with $D_h = \frac{2b}{\phi}$; and μ is the dynamic viscosity of the fluid.

Now, in the next step, the Nusselt similarity number can be calculated on the basis of a few correlations, listed in Table 1 [27–31]; additionally, calculations were performed for the model proposed by Xiu and Liu in [39].

Moreover, for the countercurrent flow, the PHE effectiveness can be calculated based on the following:

$$\varepsilon = \frac{1 - e^{-NTU\left(1 - \frac{C_{min}}{C_{max}}\right)}}{1 - \frac{C_{min}}{C_{max}} e^{-NTU\left(1 - \frac{C_{min}}{C_{max}}\right)}}; \quad for\ \frac{C_{min}}{C_{max}} < 1, \tag{15}$$

$$\varepsilon = \frac{NTU}{1 + NTU};\ for\ \frac{C_{min}}{C_{max}} = 1, \tag{16}$$

where NTU is the number of transfer units, C is the heat capacity, $C_{min} = \min(C_h,\ C_c)$, and $C_{max} = \max(C_h,\ C_c)$.

$$NTU = \frac{U\ A}{C_{min}};\ \text{for} \frac{C_{min}}{C_{max}} < 1, \tag{17}$$

where U is the heat transfer coefficient and A is the area of heat transfer. The heat capacity rate ratio C_{min}/C_{max} in the solar system is assumed to be a constant value. On the hot water circuit, the rate is variable and depends on the flow; it takes values from 0.97 for V = 0.05 L/s to 0.486 for V = 0.1 L/s.

4. Results and Discussion

In the hot channel, due to the constant flow of the working medium at 3 dm^3/min, the value of the *Re* number is slightly variable and depends primarily on the nanofluid concentration in the installation and its thermodynamic parameters and ranges from 430.25 to 328.67 for the concentration of nanofluid TiO_2:SiO_2 from 0% to 1.5% vol., respectively. In the cold channel, on the side of the domestic hot water installation, the *Re* number varies from 719 for a flow of 3 dm^3/min to 1438 for a flow of 6 dm^3/min.

Figure 3 shows how the Reynolds number changes with the concentration of the hybrid nanofluid and is inversely proportional to it. Next, for ~329 < Re_{nf} < ~430, the Nu can be expressed for models [27–31,39]. Furthermore, the dynamic viscosity of the nanofluid changes with concentration and temperature so it is safe and accurate to give a dependency in the form of Equation (13).

Figure 4a–d show how the Nusselt number changes with the *Re* and nanofluid concentration. According to data published in the literature, nanofluids consisting of two types of nanoparticles are characterised by a higher *Nu* than mono-nanofluids. An important observation is that ethylene glycol-based nanofluids also increase the *Nu* number from 10 to 32% [48]. Moreover, the *Nu* increases proportionally to the concentration of the suspension.

The range of *Re* numbers on the primary side of the installation is *Re* = 329–430 and refers to laminar flow. Figure 4 shows how the correlations available in the literature can affect the *Nu* number and, consequently, the result of the final analysis of the energy efficiency of a given system (further, Figures 5 and 6). The models defined by Akturk et al. [27], Sieder and Tate [28], Kumar et al. [29], Focke et al. [30], Okada et al. [31], and Xiu and Liu [39] were used for the analysis.

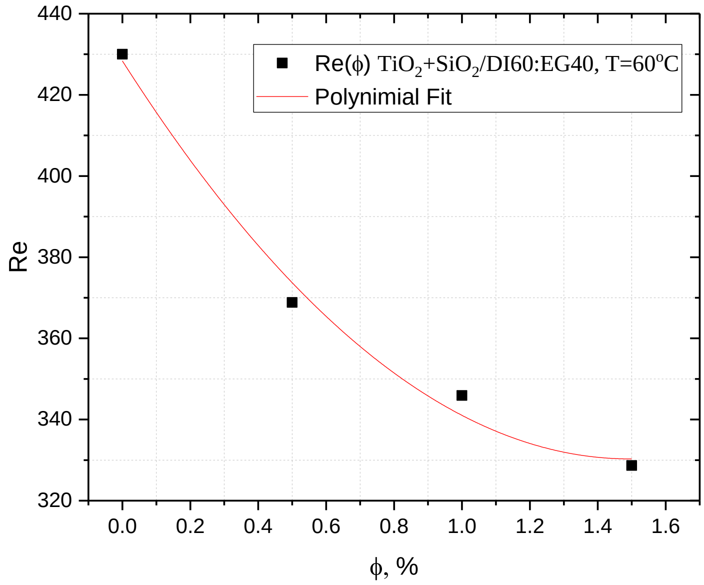

Figure 3. Reynolds number versus TiO_2:SiO_2/EG:DI nanofluid volumetric concentration.

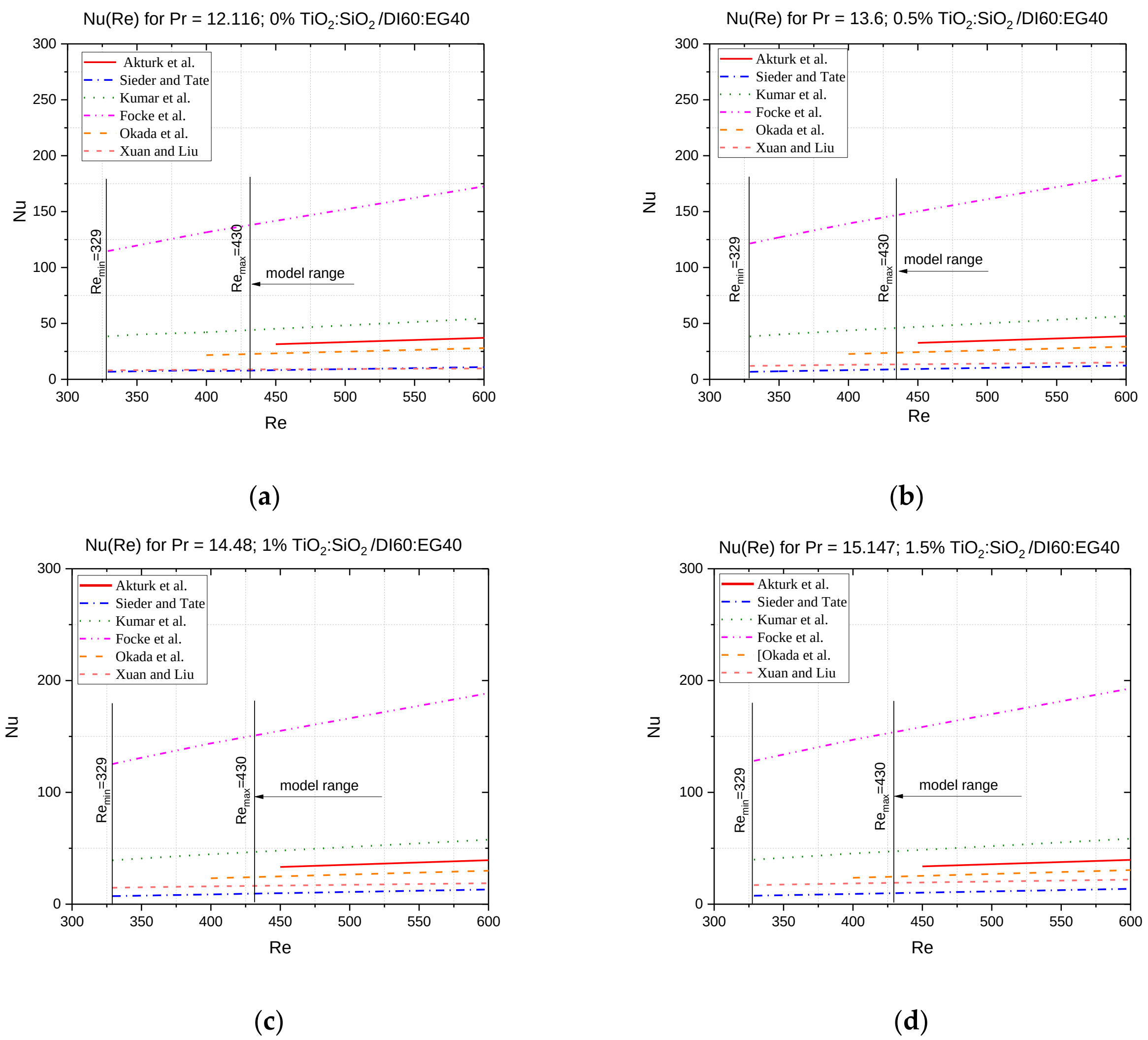

Figure 4. Variation in the Nusselt number of TiO_2:SiO_2/DI:EG hybrid nanofluid during flow through the PHE system versus Reynolds number for the following vol. concentrations: (**a**) 0%; (**b**) 0.5%; (**c**) 1.0%; (**d**) 1.5% [27–31,39].

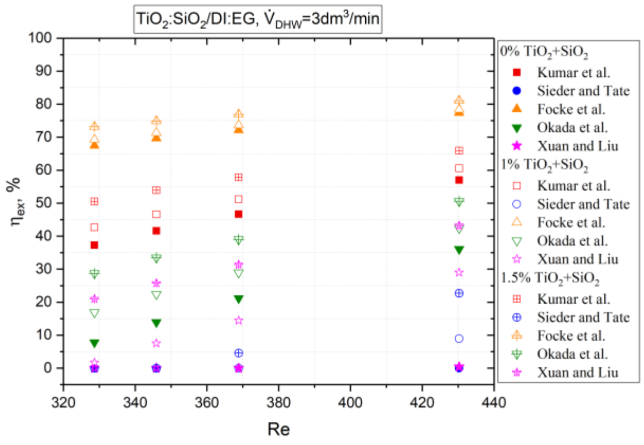

(**a**)

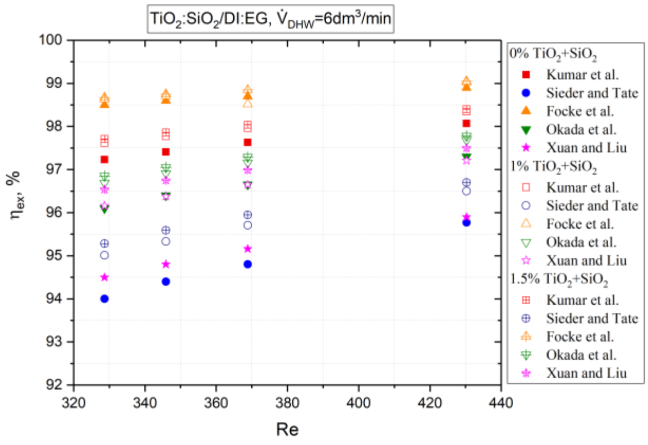

(**b**)

Figure 5. Exergy efficiency of PHE for TiO_2 + SiO_2/DI:EG hybrid nanofluid versus Reynolds number for varying Nusselt models and volumetric flow of (**a**) $\dot{V}_{nf} = 3\ \text{dm}^3/\text{min}$ and (**b**) $\dot{V}_{nf} = 6\ \text{dm}^3/\text{min}$ [28–31,39].

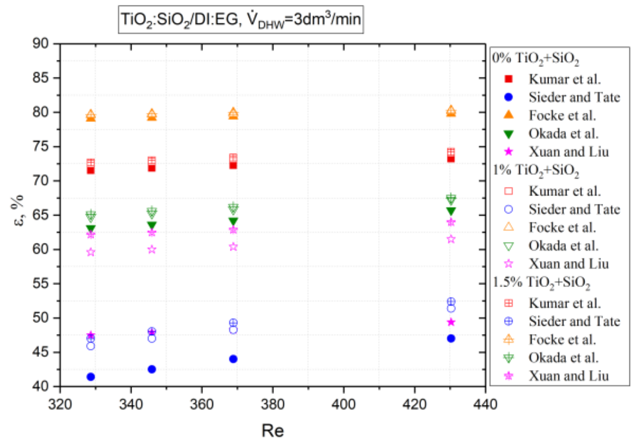

(**a**)

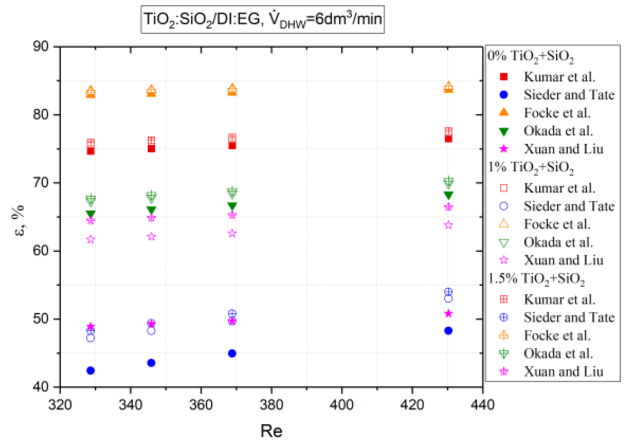

(**b**)

Figure 6. Effectiveness of PHE for TiO_2 + SiO_2/DI:EG hybrid nanofluid versus Reynolds number for varying Nusselt models and volumetric flow of (**a**) $\dot{V}_{nf} = 3\ \text{dm}^3/\text{min}$ and (**b**) $\dot{V}_{nf} = 6\ \text{dm}^3/\text{min}$ [28–31,39].

As it turns out, the models of Akturk et al. [27] and Okada et al. [31] are characterised by the highest accuracy; the standard uncertainty of type A is below $u_A < 2\%$ [27]. The average difference between the obtained results is below 10% for $Re < 1000$. However, the model [27] is validated for $Re > 450$ and [31] for $Re > 400$. For lower values, $Re < 430$, it is suggested to use the model of Kumar et al. [29], which takes average values. In terms of flows resulting from this experiment, it differs from [28] and [31] on average by 80% and 48%, respectively, and its validation has already been carried out for $Re > 10$. It should be noted that the correlation proposed by Focke et al. [24] gives results up to three times higher for the laminar range, $150 < Re < 600$; the discrepancies increase as the turbulence brews. The model of Xiu and Liu [39], for the 1.5% nanofluid, differs on average by 55% from [28], by 58% from [29], and by 87% from [30]; validation of the model [39] was performed for CuO nanofluids in the concentration range up to 2%.

The correlations by Okada [28] and Focke et al. [30] also do not take into account the influence of the liquid viscosity, which may be important in the case of nanofluids. Nanofluids are characterised by even several times higher viscosity than that of water (see Table 4). The chevron angle of the PHE [43] should also be taken into account. However, not all researchers include it as a validation parameter.

Finally, for low flows and the full range of Re = 329–430 covered by this work, it is assumed that the model of Kumar et al. [29] is proven and safe when modelling heat transfer in PHEs, as also suggested by researchers Unverdi and Islamoglu in [49]. Furthermore, the geometry of the plate and the chevron angle required in this work (which is $\beta = 30°$) coincides with the model; in [29], the influence of a viscosity is also taken into account.

The following figures show how the adopted correlation to the Nusselt number affects the final results of the exergy efficiency (see Figure 5) and the effectiveness (see Figure 6) of the PHE. The results were compared for five models, as above.

The exergy efficiency, η_{ex}, of the PHE in each case increases with concentration and the nanofluid flow through the PHE. However, if identical flow is assumed on the primary and secondary sides of the PHE, in this case 3 lpm, some of the correlations, e.g., Sieder and Tate [28], indicate very low values of η_{ex} (see Figure 5a). This means that the usefulness of the process is relatively low. When DHW is distributed and the flow through the installation is increased to 6 lpm, a visible increase in exergy efficiency is also observed, as shown in Figure 5b. The largest difference between the exergy efficiency, η_{ex}, obtained within a given concentration is 3.4% for Re = 329; the difference decreases with the flow of nanofluid through the solar installation to 2.4% for Re = 430. Therefore, it is concluded that the adoption of the correlation model on the Nusselt number does not significantly affect the final result of the PHE exergy efficiency.

The efficiency, ε, of the PHE is enhanced with the concentration of nanofluid in the solar installation and the flow on the primary side of the heat exchanger. The largest difference between the ε values obtained within a given concentration is 49% for Re = 329 but decreases with the flow of nanofluid in the solar installation to 42% for Re = 430. It is therefore concluded that the adoption of the correlation model based on the Nusselt number in this case significantly affects the efficiency of the PHE; the coefficient of determination resulting from the analysis of variance is $R^2 = 1$.

Moreover, based on the analysis of variance, the strength of the relationship between the exergy efficiency, η_{ex}, and efficiency of the PHE, ε, and the flow expressed by the Re number for the exemplary correlation of Kumar et al. [29] are determined.

Based on the statistical parameters calculated in Table 5, and the coefficient of determination of $R^2 > 0.99$, it is concluded that the exergy efficiency, η_{ex}, and the efficiency of the PHE, ε, strongly depend on the flow conditions in the PHE. However, residuals sum of squares assume much lower values for ε than in the case of η_{ex}, which may indicate a better fit of the model. In each case, the sum of squares of the residuals is much lower than the sum of squares of the regression model inputs.

Table 5. Results of regression analysis examining the influence of Re number on the efficiency, ε, and exergy efficiency, η_{ex}, of the PHE for $\dot{V}_{h,c} = 3\ \mathrm{dm^3/min}$.

Statistical Parameter	**TiO_2 + SiO_2/DI:EG Concentration**					
	Efficiency of PHE, ε			**Exergy Efficiency, η_{ex}**		
	0%	**1%**	**1.5%**	**0.5%**	**1%**	**1.5%**
Residual Sum of Squares	0.00477	0.0043	0.00408	1.71489	1.38782	1.03242
Pearson's r	0.99851	0.99844	0.99848	0.99603	0.99608	0.99605
R-Square(COD)	0.99703	0.99688	0.99696	0.99208	0.99217	0.99211
Adj. R-Square	0.99555	0.99532	0.99544	0.98812	0.98826	0.98816

As a supplement and validation of the adopted methodology, the friction factor is also computed. As the flow is laminar, the basic Hagen–Poiseuille relationship, $f = 64/Re$, was used. A graph of the relationship between the friction factor and the flow is shown below. The Hagen–Poiseuille correlation was compared with the one proposed by Alklaibi et al. [4]—see Equation (14). As is shown in Figure 7, there is a 8% difference in the obtained values.

$$f = \frac{69.95}{Re}(1+\varphi)^{-0.42} \tag{18}$$

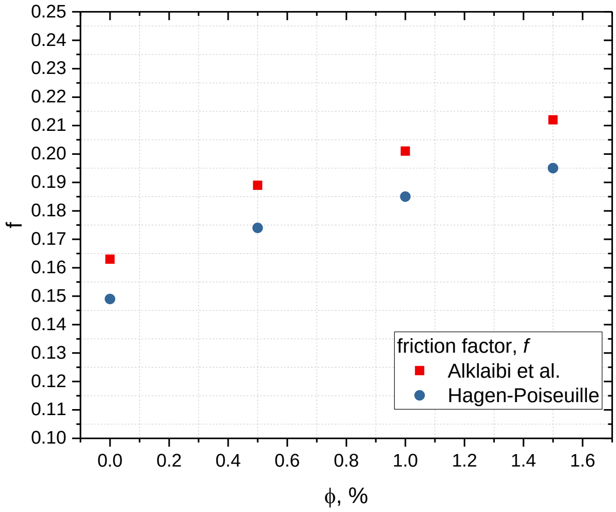

Figure 7. Friction factor versus TiO_2:SiO_2/EG:DI nanofluid concentration [4].

5. Conclusions

Plate heat exchangers are modern and effective heat transfer devices that can increase heat recovery and energy efficiency. To optimise the operation of such systems, the input factors need to be selected so that the operation is very efficient and energy-saving. Therefore, this study analyses how the correlation with the Nusselt number affects the final result of the efficiency, e, and the exergy efficiency, η_{ex}, of a chevron-type gasketed plate heat exchanger which was installed in a typical small solar installation dedicated to single-family housing. Six Nusselt correlations were considered. The heat exchanger with six plates and with a solar fluid as the TiO_2:SiO_2/EG:DI hybrid nanofluid on one side and domestic water on the other side was investigated. The experimental model assumes constant flow of the solar fluid and varies on the secondary side of the PHE—between 3 lpm and 6 lpm—and the inlet temperatures are 30 °C and 60 °C on the cold and hot sides. Most research studies that calculate the efficiency of the plate PHE assume that the nanofluid works on the secondary side of the plate heat exchanger as a coolant. This paper assumes the opposite situation. In the hot channel, due to the constant flow of the working medium, the value of the Re number is slightly variable and depends primarily on the concentration of nanofluids in the installation and its thermodynamic parameters and ranges from 430.25 to 328.67 for concentrations of TiO_2:SiO_2 nanofluid at 0–1.5% vol., respectively. Of the six analysed correlations that showed similar trends, it was concluded that for the assumed flow conditions, geometry, and chevron angle of the PHE, the model of Kumar et al. is the most accurate [29]. Furthermore, the adoption of the correlation model in the Nusselt number does not significantly affect the final result of the PHE exergy efficiency, which, according to the correlation [29], is approximately 98% for a 1.5% nanofluid. The largest difference between the η_{ex} values for a given concentration is 3.4% for Re = 329 and decreases with the flow of nanofluids in the solar installation to 2.4% for Re = 430. However, the choice of correlation on the Nusselt number significantly affects the result of the PHE efficiency result, ε; the difference between the values obtained within a given concentration is 49% for Re = 329 and decreases with the flow of nanofluid in the solar installation to 42% for Re = 430.

Funding: This research received no external funding.

Data Availability Statement: The data presented in this study are available on request from the corresponding author.

Conflicts of Interest: The author declares no conflicts of interest.

Nomenclature

A	extended heat transfer area
c	specific heat
C	heat capacity
D	hydrodynamic channel diameter
E_{conv}, E_{cond}	thermal energy exchanged by convection and conduction
f	friction factor
G	mass flow rate
h	heat transfer coefficient
k	conductive heat transfer coefficient
L_v	high of PHE
$\dot{Q}_h$	heat transfer rate
$\dot{Q}_{av}$	average heat flux
U	heat transfer coefficient
$\dot{S}_{gen}$	total entropy generation
$\dot{S}_{gen,th}$	thermal entropy
$\dot{S}_{gen,fr}$	friction entropy
T_a	ambient temperature
$T_{w,ex}$	external surface temperature
T_{in}, T_{out}	temperatures of the working fluid at the input and output of the heat exchanger
u	standard uncertainty
$\dot{V}$	volumetric flow
φ	volume or weight concentration of the suspension
ε	efficiency
ρ	density
μ	dynamic viscosity
η_{exergy}	exergy efficiency
indexes	
c	cold
h	hot
nf	nanofluid
bf	base liquid
wf	working fluid
Abbreviations	
PHE	plate heat exchanger
DI	deionised water
Nu, Pr, Re	Nusselt, Prandtl, and Reynolds numbers, respectively
NTU	Number of Transfer Units

References

1. Karapidakis, E.; Kalogerakis, C.; Pompodakis, E. Sustainable Power Generation Expansion in Island Systems with Extensive RES and Energy Storage. *Inventions* **2023**, *8*, 127. [CrossRef]
2. Mukherjee, S.; Wciślik, S.; Ebrahim, S.; Alsayegh, N. Enhancing cooling performance of a heat exchanger driven by water/alumina-silica hybrid nanofluid: Experimental results. *J. Enhanc. Heat Transf.* **2024**, *31*, 21–47. [CrossRef]
3. Zheng, D.; Du, J.; Wang, W.; Klemeš, J.J.; Wang, J.; Sundén, B. Analysis of thermal efficiency of a corrugated double-tube heat exchanger with nanofluids. *Energy* **2022**, *256*, 124522. [CrossRef]
4. Alklaibi, A.M.; Sundar, L.S.; Kotturu, V.V.; Mouli, C. Experimental investigation on the performance of hybrid Fe_3O_4 coated MWCNT/Water nanofluid as a coolant of a Plate heat exchanger. *Int. J. Therm. Sci.* **2022**, *171*, 107249. [CrossRef]
5. YousefiMiab, E.; Islami, S.B.; Gharraei, R. Feasibility assessment of using nanofluids in shell and tube heat exchanger of gas pressure reducing stations through a new developed OpenFOAM solver. *Int. J. Heat Fluid Flow* **2022**, *96*, 108985. [CrossRef]

6. Available online: https://www.sciencedirect.com/search?qs=nanofluids%2C%20plate%20heat%20exchanger&lastSelectedFacet=years (accessed on 22 September 2023).
7. Wciślik, S.; Mukherjee, S. Evaluation of three methods of static contact angle measurements for TiO_2 nanofluid droplets during evaporation. *Phys. Fluids* **2022**, *34*, 062006. [CrossRef]
8. Jafarimoghaddam, A.; Aberoumand, S. An empirical investigation on Cu/Ethylene Glycol nanofluid through a concentric annular tube and proposing a correlation for predicting Nusselt number. *Alex. Eng. J.* **2016**, *55*, 1047–1052. [CrossRef]
9. Asadi, A.; Asadi, M.; Rezaniakolaei, A.; Rosendahl, L.A.; Afrand, M.; Wongwises, S. Heat transfer efficiency of Al_2O_3-MWCNT/thermal oil hybrid nanofluid as a cooling fluid in thermal and energy management applications: An experimental and theoretical investigation. *Int. J. Heat Mass Transf.* **2018**, *117*, 474–486. [CrossRef]
10. Wciślik, S. Efficient Stabilization of Mono and Hybrid Nanofluids. *Energies* **2020**, *13*, 3793. [CrossRef]
11. Okonkwo, E.C.; Wole-Osho, I.; Almanassra, I.W.; Abdullatif, Y.M.; Al-Ansari, T. An updated review of nanofluids in various heat transfer devices. *J. Therm. Anal. Calorim.* **2021**, *145*, 2817–2872. [CrossRef]
12. Wciślik, S. A simple economic and heat transfer analysis of the nanoparticles use. *Chem. Pap.* **2017**, *71*, 2395–2401. [CrossRef]
13. Mukherjee, S.; Wciślik, S.; Khadanga, V.; Mishra, P.C. Influence of nanofluids on the thermal performance and entropy generation of varied geometry microchannel heat sink. *Case Stud. Therm. Eng.* **2023**, *49*, 103241. [CrossRef]
14. Mercan, H. Chapter 3-Thermophysical and rheological properties of hybrid nanofluids. In *Hybrid Nanofluids for Convection Heat Transfer*; Ali, H.M., Ed.; Academic Press: Cambridge, MA, USA, 2020; pp. 101–142. [CrossRef]
15. Wohld, J.; Beck, J.; Inman, K.; Palmer, M.; Cummings, M.; Fulmer, R.; Vafaei, S. Hybrid Nanofluid Thermal Conductivity and Optimization: Original Approach and Background. *Nanomaterials* **2022**, *12*, 2847. [CrossRef]
16. Fattahi, M.; Khakrah, H.; Jamalabadi, M.Y.A.; Bagheri, N.; Ross, D. Cooling of an electronic package using lattice Boltzmann/finite volume method with experimental rheological/thermal analysis of hybrid nanofluid properties. *J. Mol. Liq.* **2020**, *299*, 112143. [CrossRef]
17. Akhgar, A.; Toghraie, D. An experimental study on the stability and thermal conductivity of water-ethylene glycol/TiO_2-MWCNTs hybrid nanofluid: Developing a new correlation. *Powder Technol.* **2018**, *338*, 806–818. [CrossRef]
18. Desisa, T.R. Experimental and numerical investigation of heat transfer characteristics in solar flat plate collector using nanofluids. *Int. J. Thermofluids* **2023**, *18*, 100325. [CrossRef]
19. Nartowska, E.; Styś-Maniara, M.; Kozłowski, T. The Potential Environmental and Social Influence of the Inorganic Salt Hydrates Used as a Phase Change Material for Thermal Energy Storage in Solar Installations. *Int. J. Environ. Res. Public Health* **2023**, *20*, 1331. [CrossRef] [PubMed]
20. Nkurikiyimfura, I.; Wang, Y.; Safari, B.; Nshingabigwi, E. Electrical and thermal performances of photovoltaic/thermal systems with magnetic nanofluids: A review. *Particuology* **2021**, *54*, 181–200. [CrossRef]
21. Mehdizadeh-Fard, M.; Pourfayaz, F.; Maleki, A. Exergy analysis of multiple heat exchanger networks: An approach based on the irreversibility distribution ratio. *Energy Rep.* **2021**, *7*, 174–193. [CrossRef]
22. Tong, Y.; Lee, H.; Kang, W.; Cho, H. Energy and exergy comparison of a flat-plate solar collector using water, Al_2O_3 nanofluid, and CuO nanofluid. *Appl. Therm. Eng.* **2019**, *159*, 113959. [CrossRef]
23. Ehyaei, M.A.; Ahmadi, A.; Assad, M.E.H.; Hachicha, A.A.; Said, Z. Energy, exergy and economic analyses for the selection of working fluid and metal oxide nanofluids in a parabolic trough collector. *Sol. Energy* **2019**, *187*, 175–184. [CrossRef]
24. Iranmanesh, S.; Silakhori, M.; Naghavi, M.S.; Ang, B.C.; Ong, H.C.; Esmaeilzadeh, A. Using Graphene Nanoplatelets Nanofluid in a Closed-Loop Evacuated Tube Solar Collector—Energy and Exergy Analysis. *J. Compos. Sci.* **2021**, *5*, 277. [CrossRef]
25. Orzechowski, T.; Stokowiec, K. Quasi-stationary phase change heat transfer on a fin. *EPJ Web Conf.* **2016**, *114*, 02086. [CrossRef]
26. Purohit, N.; Purohit, V.A.; Purohit, K. Assessment of nanofluids for laminar convective heat transfer: A numerical study. *Eng. Sci. Technol. Int. J.* **2016**, *19*, 574–586. [CrossRef]
27. Akturk, F.; Sezer-Uzol, N.; Aradag, S.; Kakac, S. Experimental investigation and performance analysis of gasketed-plate heat exchangers. *J. Therm. Sci. Technol.* **2015**, *35*, 43–52.
28. Sieder, E.N.; Tate, G.E. Heat transfer and pressure drop of liquids in tubes. *Ind. Eng. Chem.* **1936**, *28*, 1429–1439. [CrossRef]
29. Kumar, H. *Evaporation in Plate Heat Exchangers*; AIChE: New York, NY, USA, 1993.
30. Focke, W.W.; Zacharides, J.; Oliver, I. The effect of the corrugation inclination angle on the thermohydraulic performance of the plate heat exchangers. *Int. J. Heat Mass Transf.* **1985**, *28*, 1469–1479. [CrossRef]
31. Okada, K.; Ono, M.; Tomimura, T.; Okuma, T.; Konno, H.; Ohtani, S. Design and heat transfer characteristics of a new plate heat exchanger. *Heat Transf. Jpn. Res.* **1972**, *1*, 90–95.
32. Kakac, S.; Liu, H. Heat Exchangers. In *Selection, Rating and Thermal Design*, 2nd ed.; CRC Press: Boca Raton, FL, USA, 2002.
33. Neagu, A.A.; Koncsag, C.I.; Barbulescu, A.; Botez, E. Calculation methods for gasket plate heat exchangers used in vegetable oil manufacture. *Comp. Study Rev. Chim.* **2015**, *66*, 1504–1508.
34. Al zahrani, S.; Islam, M.S.; Saha, S.C. A thermo-hydraulic characteristics investigation in corrugated plate heat exchanger. *Energy Procedia* **2019**, *160*, 597–605. [CrossRef]
35. Yashawantha, K.M.; Gurjar, G.; Vinod, A.V. Low Temperature Heat Transfer in Plate Heat Exchanger Using Ethylene Glycol–Water Based Al_2O_3 Nanofluid. *Int. J. Thermophys.* **2021**, *42*, 90. [CrossRef]
36. Guzman-Urbina, A.; Fukushima, K.; Ohno, H.; Fukushima, Y. Deriving local Nusselt number correlations for heat transfer of nanofluids by genetic programming. *Int. J. Therm. Sci.* **2023**, *192*, 108382. [CrossRef]

37. Vajjha, R.S.; Das, D.K.; Kulkarni, D.P. Development of new correlations for convective heat transfer and friction factor in turbulent regime for nanofluids. *Int. J. Heat Mass Transf.* **2010**, *53*, 4607–4618. [CrossRef]
38. Xuan, Y.; Li, Q. Investigation on convective heat transfer and flow features of nanofluids. *J. Heat Transf.* **2003**, *125*, 151–155. [CrossRef]
39. Li, Q.; Xuan, Y.; Jiang, J.; Xu, J.W. Experimental investigation on flow and convective heat transfer feature of a nanofluid for aerospace thermal management. *J. Astronaut.* **2005**, *26*, 391–394.
40. Lai, W.Y.; Duculescu, B.; Phelan, P.E.; Prasher, R.S. Convective heat transfer with nanofluids in a single 1.02-mm tube. In Proceedings of the ASME International Mechanical Engineering Congress and Exposition (IMECE), Chicago, IL, USA, 5–10 November 2006; pp. 65–76.
41. Chatys, R.; Orman, Ł.J. Technology and properties of layered composites as coatings for heat transfer enhancement. *Mech. Compos. Mater.* **2017**, *53*, 351–360. [CrossRef]
42. Orman, Ł.J.; Chatys, R. Heat transfer augmentation possibility for vehicle heat exchangers. In Proceedings of the 15th International Conference "Transport Means", Kaunas, Lithuania, 20–21 October 2011; pp. 9–12.
43. Kumar, S.; Singh, S.K.; Sharma, D. A Comprehensive Review on Thermal Performance Enhancement of Plate Heat Exchanger. *Int. J. Thermophys.* **2022**, *43*, 109. [CrossRef]
44. Gut, J.A.W.; Pinto, J.M. Optimal configuration design for plate heat exchangers. *Int. J. Heat Mass Transf.* **2004**, *47*, 4833–4848. [CrossRef]
45. Zainon, S.N.M.; Azmi, W.H.; Hamisa, A.H. Thermo-physical Properties of TiO_2-SiO_2 Hybrid Nanofluids Dispersion with Water/Bio-glycol Mixture. *J. Phys. Conf. Ser.* **2021**, *2000*, 012003. [CrossRef]
46. Viessmann Technical Guide. VITOSOL Flat-Plate Collectors and Vacuum Tube Collectors Flat and Pitched Roof Installation, and Wall Mounting. *5822440 GB. May 2018.* Available online: https://viessmanndirect.co.uk/files//faa19e98-f0eb-4b23-98a7-aa3201061e16/1805%20Vitosol%20Technical%20Guide%205822440VPA00013_1.PDF (accessed on 28 June 2023).
47. Gilliland, M.W. *Energy Analysis: A New Public Policy Tool*; Westview Press: Boulder, CO, USA, 1978; p. 101.
48. Upadhyay, S.; Chandra, L.; Sarkar, J. A generalized Nusselt number correlation for nanofluids, and look-up diagrams to select a heat transfer fluid for medium temperature solar thermal applications. *Appl. Therm. Eng.* **2021**, *190*, 116469. [CrossRef]
49. Ünverdi, M.; Islamoglu, Y. Characteristics of heat transfer and pressure drop in a chevron-type plate heat exchanger with Al_2O_3/water nanofluids. *Therm. Sci.* **2017**, *21*, 97. [CrossRef]